

P and SH velocity structure in the upper mantle beneath Northeast China: Evidence for a stagnant slab in hydrous mantle transition zone

Juan Li ^{a,*}, Xin Wang ^a, Xiujiao Wang ^a, David A. Yuen ^{b,c}

^a Key Laboratory of the Earth's Deep Interior, Institute of Geology and Geophysics, Chinese Academy of Sciences, 100029 Beijing, China

^b Department of Earth Sciences, University of Minnesota, Minneapolis, MN 55455, USA

^c School of Environment Sciences, China University of Geosciences, 430074 Wuhan, China

ARTICLE INFO

Article history:

Received 25 October 2012

Received in revised form

19 February 2013

Accepted 23 February 2013

Editor: P. Shearer

Available online 21 March 2013

Keywords:

mantle transition zone structure

waveform modeling

seismic wave speed

northwestern Pacific subduction zone

stagnant slab

water bearing mantle transition zone

ABSTRACT

Using high-dense regional body waves for three deep earthquakes that occurred around Russia–China border, we investigate both S and P wave velocity structures in the mantle transition zone beneath Northeast China and northern part of North China Craton, where the northwestern Pacific plate is imaged to subhorizontally lie above the 660-km discontinuity. We observe an increasing trend of S–P travel time residuals along the epicentral distance within a distance range of 11–16.5°, indicating a velocity anomaly in MTZ. We seek the simplest model that explains the observed broadband waveforms and relative travel times of triplication for a confined azimuth sector. Both SH and P data suggest a $\sim 140 \pm 20$ km high velocity layer lying above a slightly depressed and broad 660-km discontinuity. Shear velocity reduction of $\sim 2.5\%$ in the deeper part of the transition zone is required to compensate for the significantly large relative time between AB and CD triplicate branches and the increased trending of S–P travel time residuals as well. The MTZ, as a whole, is featured by low shear velocity and high V_p/V_s ratio. A water-rich mantle transition zone with 0.2–0.4 wt% of H₂O may account for the discrepancy between the observed V_p and V_s velocity structures. Our result supports the scenario of a viscosity-dominated stagnant slab with an increased thickness of ~ 140 km, which was caused by the large viscosity contrast between the lower and upper mantles. The addition of water and eastward trench retreat might facilitate stagnation of the subducting Pacific slab beneath Northeast China.

© 2013 Elsevier B.V. All rights reserved.

1. Introduction

Seismic structure of the mantle transition zone (MTZ), a region connecting the upper and lower mantles, is important for better understanding of how mantle works as a thermal–chemical engine. The interaction between the upper mantle discontinuities and the subducting lithosphere results in a heterogeneous MTZ. A depressed 660-km discontinuity (hereafter referred to as the 660) is generally expected in the cold subduction regions due to the negative Clapeyron slope of the postspinel transformation (e.g. Ito and Takahashi, 1989). The undulation of the discontinuities can be regarded as a sensitive thermometer in the Earth's deep mantle.

One ideal place to study the interaction between a subducting slab and the 660 is northeast China (Fig. 1), where the subducted Pacific slab seems to be lying sub-horizontally in the MTZ (Li and

in MTZ structure, yielding ambiguous interpretations about the

trench, and the exact same station-event geometries for P and S waves allow a tight constrain in both kinds of wave velocity near the 660 beneath the northwestern Pacific subduction zone.

3. Travel time anomalies associated with MTZ

Travel time of body waves along various paths offers the most direct information for velocity variations in the mantle (e.g. Molnar and Chen, 1984). We first applied an initial but direct travel time analysis for both S and P waves to get the first-order impression of existence of an anomaly structure associated with MTZ. We checked both horizontal components to make sure the polarities of signals are consistent with each other (Niu and Li, 2011; Li and Niu (2010)). We then removed the instrumental response and applied band-pass filters of 0.04–1 Hz and 0.04–0.5 Hz to vertical and transversal displacements, respectively. We measured first arrivals of S and P waves from vertical and transversal components for all available records in the regional distance. To quantify the effect of upper mantle anisotropy, we also handpicked first arrival time from radial components, and the arrival time difference between SH and SV is generally smaller than 0.2 s.

We noticed that two GSN stations – XAN (34.03°N, 108.92°E) and BJT (40.02°N, 116.17°E) – are located within the constructed fan-shape region. For a good calibration and comparison, we downloaded seismic waveforms from IRIS and epicentral information from EHB catalog for another three moderate deep earthquakes which occurred near the same region, and handpicked their arrival times (Fig. 1).

Fig. 2a shows P and S wave time residuals relative to model iasp91 for events 20080519, 20090716 and another three events. The SNR of vertical component of event 20081022 is low, and no first P arrivals can be clearly identified. A total of 95 and 88 records are retained for events 20080519 and 20090716, respectively. We analyzed those arrivals before the CD branch cross-overs AB for the reason that the first arrival of AB phase for P and SH waves has almost identical ray paths through the MTZ. To minimize possible scatter due to differences in velocities beneath station, we calculated S–P travel time residuals, which are the differences between the observed and calculated intervals between S wave and P wave arrival time (Fig. 2b).

The most obvious feature in these data is the enormous scatter in S time residuals, which characterizes almost all studies of S wave residuals. For distance shorter than 10°, the P time residuals are around 1.5 s, while the values of S wave are ~2–3 s, indicating contribution from the heterogeneity in the crust or shallow upper mantle. A systematical larger time residuals are observed for event 20090716 at shorter epicentral distances, which might be caused partly by the uncertainty of focal depth. Within distance range of 10–17°, the P travel time residuals range generally from –0.5 to 2 s with an average value of ~1 s. The residuals of S wave are much larger, ranging between 0.5 and 3.8 s (Fig. 2a). It has

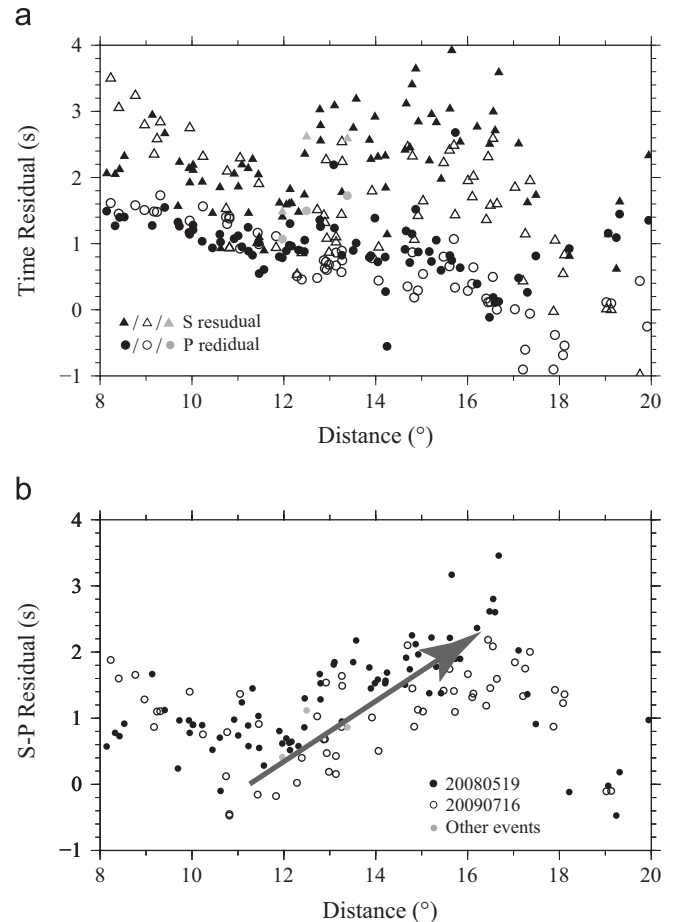


Fig. 2. P and S travel-time residuals (a) and S–P travel-time residuals (b) relative to the model iasp91 are shown with variation of epicentral distance. (a) Data for events 20080519 and 20090716 are handpicked from regional seismic networks, which are marked by solid and hollow symbols, respectively. Arrival times for two GSN stations of other deep events are marked by gray symbols. (b) Solid, hollow and gray dots indicate S–P travel-time residuals for events 20080519, 20090716, and other events, respectively. An increasing trend of S–P residuals can be obviously seen within the distance range of 11–16.5

been shown that even for the Pn and Sn waves, which travel thoroughly through the shallow upper mantle, the observed residual time beneath east China can be several seconds, and the station correction can be as large as ~2–3 s (Pei et al., 2007). Despite the large scattered data, however, there is an obvious increasing trend of S–P residuals (Fig. 2b) within epicentral distance of 11–16.5°. For event 20080519, the average value of S–P differential time residuals at distances < 11° is 0.7 s, and then it increases from ~0.3 s to a peak value of ~2.8 s at distance ~16.5°. Despite relatively low SNR, the S–P travel time residual of

event 20090716 shows the same increasing trend within epicentral distance of 11–17°.

In general, S–P travel time residuals are caused by the integrated velocity anomalies along ray paths from the source to the receiver. We notice that values of S–P residuals are closely related to the turning depth of rays. The deeper the turning depth is, the longer the ray travels through the MTZ. All S–P residuals larger than 2 s are from rays turning in the deeper MTZ. We thus infer that the increasing trend of S–P residual beyond 11° is caused by the anomaly structure in the MTZ: either the shear velocity is relatively low, or the P wave velocity is relatively faster, which will be further explored in regional triplication waveform modeling. Around epicentral distance $\sim 16.5^\circ$, CD branch of triplication phase, which dives in the upper lower mantle, becomes the first arrival and terminates the increasing trend of S–P time residuals (Fig. 2b). We emphasize that in our study, the absolute travel time is not used to constrain the deep MTZ structure; however, the S–P residual analysis gives us a simple and effective way to detect seismic velocity structure anomaly associated with the deep upper mantle to the first order.

4. Triplication waveform modeling

Triplication waveform modeling has been widely applied to constrain mantle structure (e.g. Grand and Helmberger, 1984; Wang and Yao, 1991; Tajima and Grand 1995, 1998; Brudzinski and Chen, 2000, 2003; Song et al., 2004). Due to sporadic distribution of seismic instrumentations, most previous studies were based on individual seismogram analysis, which is hard to resolve the trade-off between the interface depth and velocity variation. With the rapidly increasing installation of broadband seismic stations,

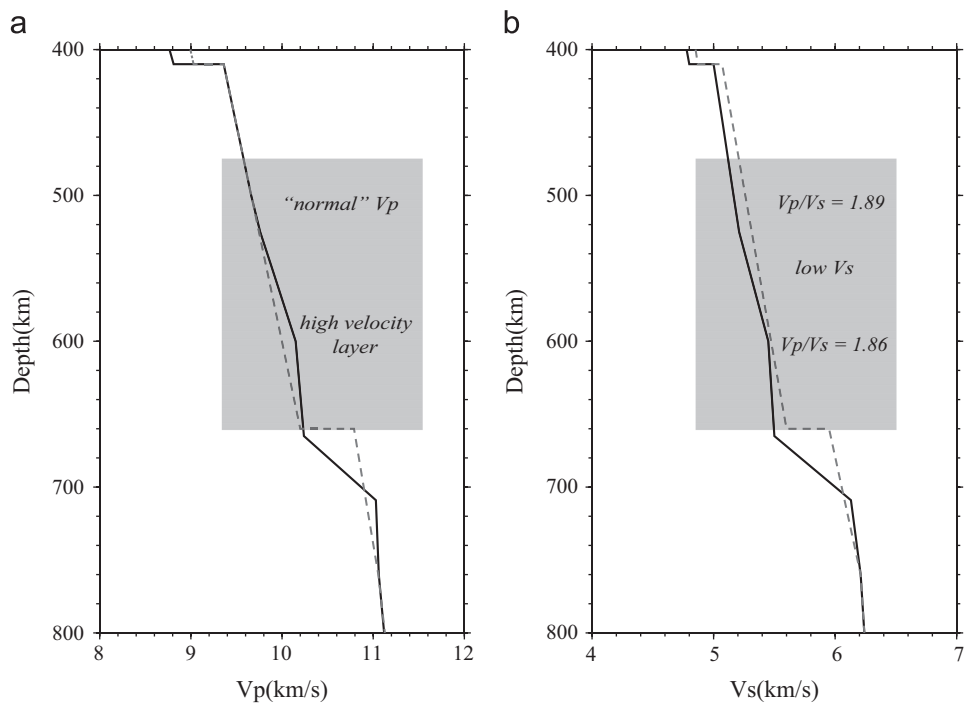


Fig. 4.

).

travel time fitting, but not the triplication waveform modeling, and thus is less well constrained.

Consistent with P velocity structure, our preferred shear velocity model also shows the presence of a high velocity ($\sim 2\%$) anomaly with thickness $\sim 140 \pm 20$ km lying above the little depressed 660 (Fig. 4b). A broad 660-km discontinuity with thickness $\sim 44 \pm 6$ km is required to explain the later appearance of CD phase. The most intriguing feature is that, in contrast to the “normal” P velocity in the MTZ, the S velocity in the MTZ is rather low relative to iasp91 as a whole. Such feature casts significant constraint on the composition and thermal anomaly in the deeper MTZ which will be discussed in the following sections.

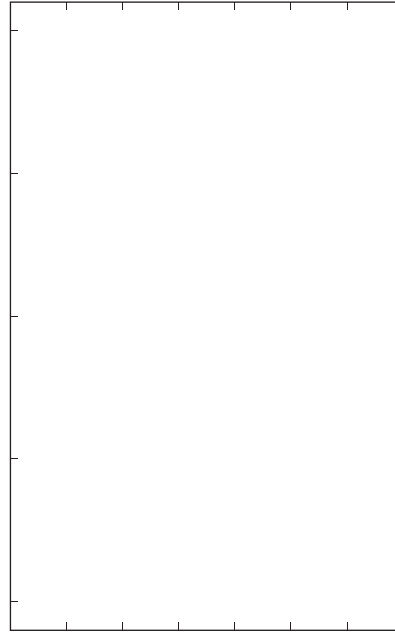
5. Discussion and interpretations

We simultaneously investigated P and S wave velocities in the deep MTZ beneath northeast China and northern North China Craton by triplication waveform modeling from three deep earthquakes. Several consistent prominent features have been detected in both P and S wave velocity structures. Uncertainty estimation of the key values associated with the structure, e.g. thickness of the high velocity layer, thickness of the broad 660, and velocity variation can be found in [Section 2 of Supplementary material](#).

We see some mismatch between the synthetic and observed waveforms. Due to the nonuniqueness of the inversion problem, we could not rule out possibility of a better resolved model; however, the striking features in the records, like extended AB branch, shortened CD branch and “broad BOD”, are well captured by the preferred models. We argue that lateral velocity heterogeneity might contribute to this inconsistency of the waveforms.

We further estimated effects of 3D velocity structure as imaged by seismic tomography on the relative travel time between the triplicate phases. We assumed a 2D raypath and counted the cumulative travel time anomalies caused by the structure (Li et al., 2008). We used P wave velocity model of Fukao et al. (2001) and an S wave velocity model converted from the P model with a scaling

relationship of $\delta \ln V_s / \delta \ln V_p = 1.6$ (Karato and Karki, 2001). The absolute travel time correction for triplicate P wave is generally ~ -1 s. For example, the AB and CD phase travel time corrections between event 20080519 and station BU.LAY (lon: 114.98° , lat: 39.51°) are -0.9 s and -1.1 s, respectively. The time correction for S phase is a little larger with values ~ -1.6 s and -1.9 s. The correction for different travel time between AB and CD phases for P and S type waves, however, is generally trivial, usually < 0.3 s, which is smaller than the assum



be constrained well. This may also explain why their synthetic waveforms match the observed vertical wiggles at further distance much better than at shorter distance.

Wang et al. (2006) applied SH waveform modeling to northeast Asia and obtained shear velocity structure “Asia” from two deep earthquakes using a large-aperture seismic array. One of the most important inferences of their results is that a lateral variation of shear velocity is not significant throughout eastern Asia. A significant depression of the 660 to 730 km was introduced, resulting in a further terminal distance of AB phase at 32° as shown in Fig. 6b. The location of O point is shifted 3° further also. Especially, the large value of relative time difference between AB and CD phases after distance $\sim 18^\circ$ could not be matched well. Recent waveform modeling has discovered that lateral velocity variation beneath northeast China and east China is significant as seen from tomographic images (Wang and Niu, 2010; Huang and Zhao, 2006; Li and van der Hilst, 2010). We argue that limitation of earlier data, lateral variation of the MTZ, and subtle effect of variation in physical properties on P and S velocities might contribute to the discrepancy.

5.2. Subduction related high velocity layer

Generally, seismic wave speed in the MTZ mainly reflects variation in thermal or compositional anomaly. P velocity models from Tajima and Grand (1998), Wang and Niu (2010) and Wang and Chen (2009) showed a low gradient high velocity layer at the base of the upper mantle, but with varied thickness. Both P and S wave velocity structures in our study, for the first time, show a quite consistent feature of a high velocity layer with thickness $\sim 140 \pm 20$ km just atop the 660. The velocity gradient increases at depth ~ 525 km with values of $5.2 \times 10^{-3} \text{ km s}^{-1} \text{ km}^{-1}$ and $4.2 \times 10^{-3} \text{ km s}^{-1} \text{ km}^{-1}$ for P and S waves, respectively. The gradient decreased to a very low value at depth around 600 km, constituting the lower part of the high velocity layer. This feature is robust since triplication for all the three events with different

epicentral depths and focal mechanisms shows a consistent feature of a long extension of cusp-B in both P and SH waveforms. We regard that the overall feature of the high velocity layer is in agreement with the tomographic image (e.g. Van der Hilst et al., 1991; Huang and Zhao, 2006) in which a stagnant slab lying horizontally in the MTZ, and the thickness of slab trapped in the MTZ is estimated to be ~ 140 km, which could not be constrained from seismic tomographic images.

The observed P and S velocity anomalies can be converted to a temperature deficit if assuming that the velocity variations are purely of thermal origin. The average P and S velocity anomalies relative to the linear trend of the velocity throughout the MTZ are $\sim 0.8\%$ and 1.1% , respectively, with the maximum value of 1.5% and 2.2% at depth ~ 600 km. Taking the temperature derivative of -6.0 to $-7.8 \times 10^{-5} \text{ K}^{-1}$ and -4.1 to $-4.5 \times 10^{-5} \text{ K}^{-1}$ for S and P velocities (Cammarano et al., 2003) respectively, we can estimate that the observed velocity anomaly corresponds to a ~ 140 – 200 K temperature variation.

5.3. A velocity transitional 660-km discontinuity

The velocity transitional 660-km discontinuity, or a “broad 660” beneath northeast China, is first examined in Wang and Niu’s work (2010) through a set of regional P waveform investigations. Here both P and SH waveform modeling show a consistent feature of a transitional 660 with thickness $\sim 44 \pm 6$ km, which is 6 km thinner than that of Wang and Niu (2010). This feature is mainly constrained by the emerging distance of cusp-C, which is most sensitive to velocity gradient at the top of the lower mantle. As shown by synthetic waveform modeling, the CD phase will appear at a shorter distance for a sharp discontinuity due to the effective wave refraction (Fig. S1).

The observed velocity transitional 660, which extends from 665 to 709 km is hard to be explained by a solely postspinel transformation. The decomposition of ringwoodite occurs at ~ 23 GPa in a very

wadsleyite (Inoue et al., 2010). Huang et al. (2005) estimated from electric conductivity observation that water content in the MTZ beneath northeast China is around 0.1–0.3 wt%, which is quite consistent with our seismological estimation. Nevertheless, how water is transported and stored in the MTZ is still a question. The phase-B or phase-D decomposition of an ancient stagnant slab might be the source of water (Kuritani et al., 2011; Zhao et al., 2009).

5.5. Implication for stagnation of subducting Pacific slab

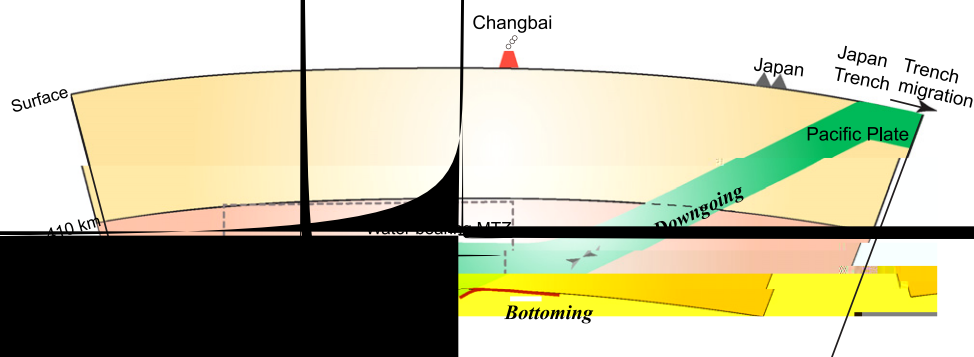
It has long been assumed that positive thermal buoyancy associated with the postspinel phase transition plays an important role in preventing slab penetration into the lower mantle. Numerical simulation of mantle convection showed that a two-layered convection can be realized provided that there is a large absolute value of Clapeyron slope (Christensen and Yuen, 1984). Recent high pressure and high temperature experiments, however, suggest that the Clapeyron slope for the postspinel transformation in anhydrous pyrolite is gentle with a value of -1 MPa/K, instead of the previously estimated range of -2 to -3 MPa/K (e.g. Katsura et al., 2003; Fei et al., 2004). With the addition of water, this value becomes more controversial (e.g. Litasov et al., 2005), and the Clapeyron slope is even proposed to be positive. In Fig. 7, we estimated the stress distribution along the slab using the CMT focal mechanism solutions of intermediate-depth and deep earthquakes that occurred after year 1990. The result clearly shows that beneath the Japan trench, the compressional stress axes of almost all deep earthquakes are parallel or sub-parallel to the down-dip motion of the slab, indicating a compression dominated regime in the subducting slab, which has also been suggested by Zhao et al. (2011). Experimental study on the grain growth of ringwoodite (Yamazaki et al., 2005) indicated that ringwoodite in a cold subducting slab has fine grain size and deforms dominantly by diffusion creep with a rather low value of viscosity. Based on our deduction of a water-bearing MTZ from the combined study of S and P waveform modeling, we argued that the strong resistance caused by the large viscosity of the lower mantle acted on the slab resulted in the strong compressional stress. The rheological weakened slab is easily bent and deformed above the 660, and formed a kind of viscosity-dominated stagnation.

To obtain a complete picture of the slab behavior around the 660, we compiled previous studies on topography of the 660 beneath northeast China. The white dashed line in Fig. 1 marks the profile where undulation of the 660 is mapped in detail by the source-sided S-to-P converted waves (Li et al. 2008). To the east of

the profile where the subducting slab has not reached the discontinuity, the 660 is almost flat, while it changed sharply west of $\sim 131^\circ\text{E}$, with a maximum depression of 20 km reported at the west end of the studied sampling point (Figs. 1 and 8). Further west, a maximum of 30–35 km depression was mapped just to the northeast corner of our study region (orange shadow in Fig. 1) using receiver function technique. We thus attain a more clear and consistent image of the behavior of the subducting Pacific slab beneath Japan trench. We divide the subducting slab into three parts: downgoing, bottoming and stagnant parts. During the downgoing part, no change of the 660-km discontinuity occurred since there is no interaction between the slab and the boundary. When the slab encountered the 660 around $\sim 131^\circ\text{E}$, the 660 deflected sharply due to the coldness of the slab, with the largest depression corresponding to the coldest core of the slab, and then formed the bottoming part. Due to the large viscosity contrast between the slab and lower mantle, the slab bent, extended westward and stayed stagnant in the MTZ.

A slab with thickness ~ 80 – 90 km has been mapped through seismic tomographic images, which is quite consistent with an estimation of a 120 Ma year old slab. The thickness of the high velocity layer in the stagnant part, however, could not be constrained well through tomographic technique, and the high velocity anomaly seems to distribute throughout the whole MTZ (Huang and Zhao, 2006; Li and van der Hilst, 2010). Our result suggested that the stagnant slab has a thickness ~ 140 km, which seems to be 50–60 km thickened from the initial value. We argue that the large viscosity contrast between the lower and upper mantles results in the obvious thickening of slab in the stagnant part. Numerical experiments of mantle convection (Kameyama and Nishioka, 2012) show that thickening of the slab will occur near the oceanward end of stagnant slabs where they meet the 660 and bend, and it will be significant for a larger viscosity contrast and trench retreat velocity. The retreat of trench under Japan–Kurile arc from Miocene (Miller et al., 2006) revealed by Paleotectonic reconstruction studies might also facilitate the thickening of the slab.

Combined with tomographic images beneath northeast China, our results imply that the stagnant Pacific slab lies subhorizontally in a water-bearing MTZ beneath northeast China (Fig. 8). Geochemical analysis of a limit basalt samples around Changbai volcano has revealed a regional water-rich MTZ (Kuritani et al., 2011). From the distribution of turning points of CD phase (white points in Fig. 1 with distance $< 25^\circ$), which is most critical in constraining discrepancy structure between V_p and V_s , we argue that the hydrous MTZ is more widely distributed than previous



geochemical deduction. It might extend as far as 118°E, roughly corresponding to the steepest topographic gradient belt in China.

6. Conclusions

We have shown that fine-scale seismic structure in the heterogeneous MTZ can be obtained effectively from triplication waveform modeling for a set of densely distributed stations. Simultaneous modeling of S and P waveforms provides a useful way for identifying thermal or compositional anomalies associated with subduction process. A high velocity layer with thickness ~140 km is detected lying in the MTZ which corresponds to the deflected and stagnant Pacific slab. The high V_p/V_s ratio in the MTZ indicates a water-bearing MTZ, which might extend 900–1100 km westward of Changbai volcano. Our results support the scenario that due to the large resistance exerted by the lower mantle, the rheology weakened slab bends easily while encountering the 660 and then lies subhorizontally in the water-rich MTZ. Nevertheless, finite difference waveform synthetic for a 3D velocity structure should be applied to account for the lateral velocity variation, and simulation on the interaction between the 660 and the subducting slab is required for a full understanding of the geodynamic mechanism and composition of the upper mantle beneath the northwestern Pacific subduction zone.

Acknowledgments

This research is supported by NSFC (J. Li, Grant 41074034). We thank Risheng Chu and an anonymous referee for constructive and valuable comments, which improved the manuscript greatly. Thanks to Dr. Shengqiang Li of China Earthquake Administration for providing the focal mechanism solution for event 20081022 with Mw 4.7. Lingling Ye has joined the discussion and contributed to earlier work. Thanks to Prof. Fenglin Niu's discussion on travel time analysis and seismic structure beneath northeast China. We thank the Data Management Centre of China National Seismic Network at Institute of Geophysics, China Earthquake Administration and IRIS DMS, for providing seismic data. Sac2000 and GMT are used in basic data processing and plotting of some figures.

Appendix A. Supplementary materials

Supplementary data associated with this article can be found in the online version at <http://dx.doi.org/10.1016/j.epsl.2013.02.026>.

References

- Ai, Y., Zheng, T., Xu, W., Dong, D., 2003. A complex 660 km discontinuity beneath northeast China. *Earth Planet. Sci. Lett.* 212, 63–71.
- Bijwaard, H., Spakman, W., Engdahl, E., 1998. Closing the gap between regional and global travel time tomography. *J. Geophys. Res.* 103, 30055–30078.
- Brudzinski, M.R., Chen, W.P., 2000. Variations in P wave speeds and outboard earthquakes: evidence for a petrologic anomaly in the mantle transition zone. *J. Geophys. Res.* 105, 21661–21682.
- Brudzinski, M.R., Chen, W.-P., 2003. A petrologic anomaly accompanying outboard earthquakes beneath Fiji-Tonga: corresponding evidence from broadband P and S waveforms. *J. Geophys. Res.*, 108, 2299, <http://dx.doi.org/10.1029/2002JB002012>.
- Buland, R., Chapman, C.H., 1983. The computation of seismic travel times. *Bull. Seismol. Soc. Am.* 73, 1271–1302.
- Cammarano, F., Goes, S., Vacher, P., Giardini, D., 2003. Inferring upper-mantle temperatures from seismic velocities. *Phys. Earth Planet. Inter.* 138, 197–222.
- Christensen, U.R., Yuen, D.A., 1984. The interaction of a subducting lithospheric slab with a chemical or phase boundary. *J. Geophys. Res.* 89, 4389–4402.
- de Wit, R.W.L., Trampert, J., van der Hilst, R.D., 2012. Toward quantifying uncertainty in travel time tomography using the null-space shuttle. *J. Geophys. Res.* 117, B03301.
- Fei, Y., Van Orman, J., Li, J., van Westrenen, W., Sanloup, C., Minarik, W., Hirose, K., Komabayashi, T., Walter, M., Funakoshi, K., 2004. Experimentally determined postspinel transformation boundary in Mg_2SiO_4 using MgO as an internal pressure standard and its geophysical implications. *J. Geophys. Res.* 109, B02305.
- Fukao, Y., 1977. Upper mantle P structure on the ocean side of the Japan-Kurile arc. *Geophys. J. Int.* 50, 621–642.
- Fukao, Y., Widiyatoro, S., Obayashi, M., 2001. Stagnant slabs in the upper and lower mantle transition region. *Rev. Geophys.* 39, 291–323.
- Fukao, Y., Obayashi, M., Nakakuki, T., 2009. Stagnant slab: a review. *Annu. Rev. Earth Planet. Sci.* 37, 19–46.
- Gorbatov, A., Kennett, B.L.N., 2003. Joint bulk-sound and shear tomography for Western Pacific subduction zones. *Earth Planet. Sci. Lett.* 210, 527–543.
- Grand, S.P., Helmsberger, D.V., 1984. Upper mantle shear structure of North America. *Geophys. J. R. Astron. Soc.* 76, 399–438.
- Higo, Y., Inoue, T., Li, B., Irifune, T., Liebermann, R.C., 2006. The effect of iron on the elastic properties of ringwoodite at high pressure. *Phys. Earth Planet. Inter.* 159, 276–285.
- Huang, J.L., Zhao, D.P., 2006. High-resolution mantle tomography of China and surrounding regions. *J. Geophys. Res.* 111, B09305.
- Huang, X., Bai, W., Xu, Y.S., Karato, S.-i., 2005. Influence of hydrogen on electrical conductivity of wadsleyite and ringwoodite with its geodynamics implications. *Acta Petrol. Sin.* 21 (6), 1743–1748 (in Chinese).
- Ichiki, M., Baba, K., Obayashi, M., Utada, H., 2006. Water content and geotherm in the upper mantle above the stagnant slab: interpretation of electrical conductivity and seismic P-wave velocity models. *Phys. Earth Planet. Inter.* 155, 1–15.
- Inoue, T., Wada, T., Sasaki, R., Yurimoto, H., 2010. Water partitioning in the earth's mantle. *Phys. Earth Planet. Inter.* 183, 245–251.
- Irifune, T., Kubo, N., Ishiki, M., Yamasaki, Y., 1998. Phase transformations in serpentine and transportation of water into the lower mantle. *Geophys. Res. Lett.* 25, 203–206.
- Ito, E., Takahashi, E., 1989. Postspinel transformations in the system Mg_2SiO_4 – Fe_2SiO_4 and some geophysical implications. *J. Geophys. Res.* 94, 10637–10646.
- Jacobsen, S., Smyth, J., 2006. Effect of water on the sound velocities of ringwoodite in the transition zone. *Geophys. Monogr.—Am. Geophys. Union* 168, 131.
- Jacobsen, S.D., Smyth, J.R., Spetzler, H., Holl, C.M., Frost, D.J., 2004. Sound velocities and elastic constants of iron-bearing hydrous ringwoodite. *Phys. Earth Planet. Inter.* 143–144, 47–56.
- Kameyama, M., Nishioka, R., 2012. Generation of ascending flows in the Big Mantle Wedge (BMW) beneath northeast Asia induced by retreat and stagnation of subducted slab. *Geophys. Res. Lett.* 39, L10309.
- Karato, S.-i., 2011. Water distribution across the mantle transition zone and its implications for global material circulation. *Earth Planet. Sci. Lett.* 301, 413–423.
- Karato, S.-i., Karki, B., 2001. Origin of lateral variation of seismic wave velocities and density in the deep mantle. *J. Geophys. Res.* 106 (21), 771–21784.
- Katsura, T., Yamada, H., Shinmei, T., Kubo, A., Ono, S., Kanzaki, M., Yoneda, A., Walter, M.J., Ito, E., Urakawa, S., Funakoshi, K., Utsumi, W., 2003. Post-spinel transition in Mg_2SiO_4 determined by high P–T in situ X-ray diffractometry. *Phys. Earth Planet. Inter.* 136, 11–24.
- Kuritani, T., Ohtani, E., Kimura, J.-I., 2011. Intensive hydration of the mantle transition zone beneath China caused by ancient slab stagnation. *Nat. Geosci.* 4, 713–716.
- Li, C., van der Hilst, R.D., 2010. Structure of the upper mantle and transition zone beneath Southeast Asia from traveltimes tomography. *J. Geophys. Res.* 115, B07308.
- Li, J., Chen, Q.F., Vanacore, E., Niu, F.L., 2008. Topography of the 660-km discontinuity beneath northeast China: implications for a retrograde motion of the subducting Pacific slab. *Geophys. Res. Lett.* 35, L01302.
- Li, J., Niu, F., 2010. Seismic anisotropy and mantle flow beneath northeast China inferred from regional seismic networks. *J. Geophys. Res.* 115, B12327.
- Li, S.Q., 2012. Quasi-Automatic Waveform Inversion of Focal Mechanisms of Moderate and Small Earthquakes on High-Performance Cluster Computing System and Applications. PhD. Thesis (in Chinese).
- Li, X.Q., Yuan, X.H., 2003. Receiver functions in northeast China—implications for slab penetration into the lower mantle in northwest Pacific subduction zone. *Earth Planet. Sci. Lett.* 216, 679–691.
- Litasov, K.D., Ohtani, E., Sano, A., 2006. Influence of water on major phase transitions in the Earth's mantle, Earth's Deep Water Cycle. AGU, Washington, DC, pp. 95–111.
- Litasov, K.D., Ohtani, E., Sano, A., Suzuki, A., Funakoshi, K., 2005. Wet subduction versus cold subduction. *Geophys. Res. Lett.* 32, L13312.
- Miller, M.S., Kennett, B.L.N., Toy, V.G., 2006. Spatial and temporal evolution of the subducting Pacific plate structure along the western Pacific margin. *J. Geophys. Res.* 111, B02401.
- Molnar, P., Chen, W.-P., 1984. S–P wave travel time residuals and lateral inhomogeneity in the mantle beneath Tibet and the Himalaya. *J. Geophys. Res.* 89, 6911–6917.
- Niu, F., Kawakatsu, H., 1996. Complex structure of mantle discontinuities at the tip of the subducting slab beneath northeast China. *J. Phys. Earth* 44, 701–711.
- Niu, F., Li, J., 2011. Component azimuths of the CEArray stations estimated from P-wave particle motion. *Earthquake Sci.* 24, 3–13.
- Pei, S., Zhao, J., Sun, Y., Xu, Z., et al., 2007. Upper mantle seismic velocities and anisotropy in China determined through Pn and Sn tomography. *J. Geophys. Res.* 112, B05312.
- Sinogeikin, S., Katsura, T., Bass, J., 1998. Sound velocities and elastic properties of Fe-bearing wadsleyite and ringwoodite. *J. Geophys. Res.* 103, 20819–20825.

- Sinogeikin, S.V., Bass, J.D., Katsura, T., 2001. Single-crystal elasticity of γ -(Mg_{0.91}Fe_{0.09})₂SiO₄ to high pressures and to high temperatures. *Geophys. Res. Lett.* 28, 4335–4338.
- Song, A.T.-R., Helmberger, D.V., Grand, S.P., 2004. Low-velocity zone atop the 410-km seismic discontinuity in the northwestern United States. *Nature* 427, 530–533.
- Tajima, F., Grand, S.P., 1995. Evidence of high-velocity anomalies in the transition zone associated with Southern Kurile subduction zone. *Geophys. Res. Lett.* 22, 3139–3142.
- Tajima, F., Grand, S.P., 1998. Variation of transition zone high-velocity anomalies and depression of 660 km discontinuity associated with subduction zones from the southern Kuriles to Izu-Bonin and Ryukyu. *J. Geophys. Res.* 103, 15015–15036.
- Tajima, F., Katayama, I., Nakagawa, T., 2009. Variable seismic structure near the 660 km discontinuity associated with stagnant slabs and geochemical implications. *Phys. Earth Planet. Inter.* 172, 183–198.
- Tajima, F., Nakagawa, T., 2006. Implications of seismic waveforms: complex physical properties associated with stagnant slab. *Geophys Res Lett* 33, L03311.
- Van der hilst, R., Engdahl, R., Spakman, W., Nolet, G., 1991. Tomographic imaging of subducted lithosphere below Northwest Pacific Island arcs. *Nature* 353, 37–43.
- Wang, B., Niu, F., 2010. A broad 660-km discontinuity beneath northeastern China revealed by dense regional seismic networks in China. *J. Geophys. Res.* 115, B06308.
- Wang, K., Yao, Z., 1991. Upper mantle P velocity structure of southern China. *Chin. J. Geophys.* 34, 309–317 (in Chinese).
- Wang, T., Chen, L., 2009. Distinct velocity variations around the base of the upper mantle beneath northeast Asia. *Phys. Earth Planet. Inter.* 172, 241–256.
- Wang, Y., Wen, L.X., Weidner, D., He, Y.M., 2006. SH velocity and compositional models near the 660-km discontinuity beneath South America and northeast Asia. *J. Geophys. Res.* 111, B07305.
- Yamazaki, D., Inoue, T., Okamoto, M., Irifune, T., 2005. Grain growth kinetics of ringwoodite and its implication for rheology of the subducting slab. *Earth Planet. Sci. Lett.* 236, 871–881.
- Ye, L., Li, J., Tseng, T.-L., Yao, Z., 2011. A stagnant slab in a water-bearing mantle transition zone beneath northeast China: implications from regional SH waveform modelling. *Geophys. J. Int.* 186, 706–710.
- Zhao, D., Tian, Y., Lei, J., Liu, L., Zheng, S., 2009. Seismic image and origin of the Changbai intraplate volcano in East Asia: role of big mantle wedge above the stagnant Pacific slab. *Phys. Earth Planet. Inter.* 173, 197–206.
- Zhao, D., Yu, S., Ohtani, E., 2011. East Asia: seismotectonics, magmatism and mantle dynamics. *J. Asian Earth Sci.* 40, 689–709.
- Zheng, X.-F., Yao, Z.-X., Liang, J.-H., Zheng, J., 2010. The role played and opportunities provided by IGP DMC of China National Seismic Network in Wenchuan Earthquake Disaster Relief and Researches. *Bull. Seismol. Soc. Am.* 100, 2866–2872.
- Zhu, L., Helmberger, D., 1996. Advancement in source estimation techniques using broadband regional seismograms. *Bull. Seismol. Soc. Am.* 86, 1634–1641.